Redox Biology 50 (2022) 102250

Contents lists available at ScienceDirect

Redox Biology

journal homepage: www.elsevier.com/locate/redox

In vivo hydrogen peroxide diffusivity in brain tissue supports volume signaling activity

A. Ledo [a,b,*], E. Fernandes [a], A. Salvador [b,c,d], J. Laranjinha [a,b], R.M. Barbosa [a,b]

[a] Faculty of Pharmacy, University of Coimbra, Azinhaga de Santa Comba, 3000-548, Coimbra, Portugal
[b] Center for Neuroscience and Cell Biology, University of Coimbra, Rua Larga, 3004-504, Coimbra, Portugal
[c] Institute for Interdisciplinary Research, University of Coimbra, Casa Costa Alemão, 3030-789, Coimbra, Portugal
[d] CQC, Department of Chemistry, University of Coimbra, Rua Larga, 3000-535, Coimbra, Portugal

ARTICLE INFO

Keywords:
Hydrogen peroxide
Volume signaling
Diffusion
Brain

ABSTRACT

Hydrogen peroxide is a major redox signaling molecule underlying a novel paradigm of cell function and communication. A role for H_2O_2 as an intercellular signaling molecule and neuromodulator in the brain has become increasingly apparent, with evidence showing this biological oxidant to regulate neuronal polarity, connectivity, synaptic transmission and tuning of neuronal networks. This notion is supported by its ability to diffuse in the extracellular space, from source of production to target. It is, thus, crucial to understand extracellular H_2O_2 concentration dynamics in the living brain and the factors which shape its diffusion pattern and half-life. To address this issue, we have used a novel microsensor to measure H_2O_2 concentration dynamics in the brain extracellular matrix both in an *ex vivo* model using rodent brain slices and *in vivo*. We found that exogenously applied H_2O_2 is removed from the extracellular space with an average half-life of $t_{1/2} = 2.2$ s *in vivo*. We determined the *in vivo* effective diffusion coefficient of H_2O_2 to be $D^* = 2.5 \times 10^{-5}$ cm^2 s^{-1}. This allows it to diffuse over 100 μm in the extracellular space within its half-life. Considering this, we can tentatively place H_2O_2 within the class of volume neurotransmitters, connecting all cell types within the complex network of brain tissue, regardless of whether they are physically connected. These quantitative details of H_2O_2 diffusion and half-life in the brain allow us to interpret the physiology of the redox signal and lay the pavement to then address dysregulation in redox homeostasis associated with disease processes.

1. Introduction

Hydrogen peroxide – H_2O_2 – is a major biological oxidant which plays a pleiotropic role in redox regulation of cell functions. Its intracellular concentration is maintained in the steady-state low nanomolar range through regulation of production and efficient redundant removal systems [1]. H_2O_2 is a strong 2-electron oxidant, but its high activation energy renders it relatively stable and limits its reaction with most biological molecules. In the brain, this oxidant has been shown to regulate neuronal polarity, connectivity, synaptic transmission in addition to tuning of neuronal networks (reviewed in Refs. [2,3]), and redox imbalance or oxidative stress are strongly associated with neurodegeneration and can undermine deleterious neuroinflammatory responses [4]. In the striatum H_2O_2 is proposed to be released from medium spiny neurons in response to glutamate depolarization, resulting in the down-regulation of dopamine release from midbrain afferents (reviewed in Ref. [5]).

The intracellular concentration of H_2O_2 is maintained in low nM levels due to the activity of molecular sinks [6,7], while extracellular concentrations may be higher. Some reports point towards a blood plasma level as high as 1–5 μM [8], however careful experiments and critical analysis suggest that blood plasma levels of H_2O_2 may be in the low nM range, with the exception of situations such as inflammation or infection [9–11]. Also, the concentration of H_2O_2 varies in mammalian cells within different compartments: lowest [H_2O_2] is found in the cytosol (80 pM–2.2 nM), while inside the endoplasmic reticulum, 700 nM concentration has been reported [6,12,13]. Steep concentration gradients are expected to be found in the cytosol centered at H_2O_2 entry or production sites [13,14]. Although H_2O_2 can cross biological membranes through passive diffusion [15,16], sharp gradients across biomembranes were identified in the seminal work by Antunes and Cadenas [17]. Higher transport rates are afforded by several aquaporins, coined

* Corresponding author. Faculty of Pharmacy, University of Coimbra, Azinhaga de Santa Comba, 3000-548, Coimbra, Portugal.
E-mail address: analedo@ff.uc.pt (A. Ledo).

https://doi.org/10.1016/j.redox.2022.102250
Received 13 January 2022; Received in revised form 18 January 2022; Accepted 24 January 2022
Available online 26 January 2022

"peroxiporins", shown to facilitate H_2O_2 diffusion across biomembranes [18]. The occurrence of H_2O_2 transport systems across the cell membranes advances the notion that the extracellular concentration of H_2O_2 impacts dynamically on intracellular signaling pathways in neighboring cells.

Enzymes responsible for removal of H_2O_2 include peroxiredoxins (Prx) and glutathione peroxidases (GPx), both of which display high second-order rate constants in the range of 10^5-10^8 M^{-1} s^{-1} relative to H_2O_2 [19]. Peroxiredoxins can transmit the oxidizing equivalents to other target proteins, acting as redox relays in thiol-dependent H_2O_2 signaling [20]. Catalase (CAT) is a heme protein that, in its main catalytic cycle, catalyzes the 2-step dismutation of two H_2O_2 molecules to water and O_2 with no net consumption of cellular reducing equivalents [21,22]. Finally, peroxidase enzymes use H_2O_2 as a substrate to generate oxidants, as is the case of myeloperoxidase found in neutrophils that produces hypochlorous acid as part of the pathogen defense mechanism [23].

Inherent to the notion of H_2O_2 as an intercellular signaling molecule is its diffusion in the extracellular space. To understand the distribution and range of influence of a particular diffusible compound in brain tissue one must know its effective diffusion coefficient (D^*) and the relative importance of diffusion *vs* clearance processes that participate in the removal and or degradation/decomposition from the extracellular space (ECS). Diffusion in the ECS can be modified by removal across the blood brain barrier, uptake into cells or binding to receptors (concepts reviewed in Ref. [24]). Here we have investigated H_2O_2 concentration dynamics in the brain ECS in the striatum both in an acute slice preparation and *in vivo*. To this purpose we have used novel ruthenium purple modified carbon fiber microelectrodes (RP-CFM) which we have previously designed and characterized for their electrocatalytical properties towards the selective detection of H_2O_2 concentration with high spatial and temporal resolution [25]. We determined the half-life of H_2O_2 in brain tissue and used mathematical modelling to determine D^* *in vivo,* thus inferring its diffusional spread in the brain.

2. Materials and methods

Reagents and Solutions: Reagents were analytical grade and obtained from Sigma-Aldrich. Argon was provided by Air Liquide, Portugal and Carbox (95% O_2/5%CO_2) was obtain from Linde Sogas, Portugal. All solutions were prepared in ultra-pure deionized water (≥18 MΩ cm) from a Milli-Q system (Millipore Company, Bedford, MA, USA). Microelectrode *in vitro* evaluations were performed in phosphate buffered saline (PBS) with the following composition (in mM): 140 NaCl, 2.7 KCl, 8.1 Na_2HPO_4, 1.8 KH_2PO_4, pH 7.4. Media for hippocampal slice experiments was artificial cerebrospinal fluid (aCSF) composed of (in mM): 124 NaCl, 2 KCl, 25 $NaHCO_3$, 1.25 KH_2PO_4, 1.5 $CaCl_2$ and 10 D-glucose. For dissection and recovery, a modified aCSF was used to increase viability. Composition of this aCSF was (in mM): 124 NaCl, 2 KCl, 25 $NaHCO_3$, 1.25 KH_2PO_4, 0.5 $CaCl_2$, 10 $MgSO_4$, 0.2 AA, 1 GSH and 10 D-glucose. In all cases, aCSF was continuously bubbled with humidified Carbox for pH buffering (pH 7.4) and oxygenation.

Animals: All the procedures in this study were performed in accordance with the European Union Council Directive for the Care and Use of Laboratory animals, 2010/63/EU, and were approved by the local ethics committee (ORBEA) and the Portuguese Directorate-General for Food and Veterinary. A total of 21 male Wistar rats aged 8–12 weeks and weighing 300–390 g (Charles-River Laboratories, Barcelona, Spain) were used in these experiments: 6 for slices and 15 for *in vivo*. While in the animal facility, animal husbandry conditions were as follows: housed in pairs in filter-topped type III Makrolon cages in the local vivarium with controlled environmental conditions, namely a temperature of 22–24 °C, relative humidity of 45–65%, air exchange rate of 15 times per hour, 12 h light/dark cycle, and with standard rat chow diet (4RF21-GLP Mucedola, SRL, Settimo Milanese, Italy) and chlorinated water available *ad libitum*.

Carbon Fiber Microelectrode Fabrication, Modification and Evaluation: Carbon fiber microelectrodes (CFM) were fabricated as previously described [26]. Briefly, a single carbon fiber (30 μm o.d.; Textron Lowell, MA, USA) was inserted into a borosilicate glass capillary (1.16 mm i.d. and 2.0 mm o.d.; Harvard Apparatus, Holliston, MA, USA) and cleaned with acetone. Each capillary was pulled using a vertical puller (Harvard Apparatus, UK) and the protruding carbon fiber was cut to a tip length of approx. 150 μm. The electrical contact between the carbon fiber and the copper wire was provided by conductive silver paint (RS, Northants, UK). The microelectrodes were tested for general recording properties in 0.05 M PBS Lite (in mM: 10 Na_2HPO_4, 40 NaH_2PO_4, and 100 NaCl, pH 7.4) by fast cyclic voltammetry at a scan rate of 200 V s^{-1}, between −0.4 and + 1.6 V *vs* Ag/AgCl for 30 cycles.

Ruthenium purple (RP) modification of CFM was achieved as described in Ref. [25]. Briefly, a solution of 1 mM K_4 [$Ru^{II}(CN)_6$] prepared in 35 mM KCl (N_2-purged) was mixed, under vigorous stirring, with a solution of 1 mM $FeCl_3$ in 35 mM KCl (N_2-purged). The pH of the resulting colloidal suspension was adjusted to 2.0 using 1 M HCl. This solution was placed in an ultrasound bath and $RuCl_3$ was added from a 1 mM solution to give a final concentration of 20 μM. This solution was used within 4 h of preparation. Electrodeposition was carried out by potential cycling between −0.2 and + 1.0 V *vs* Ag/AgCl at a scan rate of 50 mV s^{-1}. The cycles were repeated until the redox peaks no longer increased in height. The modified CFM (CFM-RP) was rinsed with distilled water and placed in a solution of 1 mM $RuCl_3$ in 35 mM KCl. Between 2 and 4 further cycles were performed under the same conditions to ensure the stability of the deposited film. For coating with Nafion®, the tip of the CFM-RP was dipped into a 5% solution of Nafion® in aliphatic alcohols for 5 s and then dried at 100 °C for 15 min. These sensors were designated CFM-RP-Nafion®.

Preparation of Rat Striatum Slices: Following decapitation under deep anesthesia (isoflurane), the brain of the animal was rapidly removed and placed in ice-cold, Carbox bubbled modified aCSF. The cerebellum was removed, the two hemispheres were separated and mounted in the pre-chilled stage of a vibratome (Vibroslice, World Precision Instruments) and submerged in the chamber filled with ice cold modified aCSF continuously bubbled with Carbox. Brain slices containing the striatum were obtained with a thickness of 400 μm and transferred to a pre-incubation chamber (BSC-PC; Harvard Apparatus) filled with modified aCSF. Slices were allowed to recover under these conditions for at least 1 h prior to recording.

Recording H_2O_2 in Rat Striatal Slices: An individual slice was placed in a recording chamber (BSC-BU with BSC-ZT top, Harvard Apparatus) and perfused with aCSF continuously bubbled with humidified Carbox and at a flow rate of 1.5–2 mL min^{-1}. The temperature of the chamber was maintained at 32 °C (temperature controller model TC-202A, Harvard Apparatus). A recording array comprised of a CFM-RP-Nafion® and a CFM mounted at a tip-to-tip distance of 100 μm was lowered into the tissue with the aid of a micromanipulator so as to guarantee that the totality of the active surface was in the tissue core. Recording of the reduction current was initiated and once a stable baseline was obtained, an H_2O_2 solution (1 mM in aCSF) was pressure ejected (10 Psi, 1s) via a Picospritzer II (General Valve, Fairfield, NJ) through a pulled micropipette, placed between the two working electrodes.

2.1. In vivo recording of hydrogen peroxide in the brain of anesthetized rats

The experimental setup used for amperometric monitoring of H_2O_2 *in vivo* in anesthetized rats was similar to that used in previous studies [27]. Briefly, an animal was anesthetized with urethane 1.25 g kg^{-1} (i.p.) and placed in a stereotaxic apparatus. Body temperature was maintained at 37 °C with a heated pad coupled to a Gaymar Heating Pump (Braintree Scientific, Inc., USA). The skull was exposed by a midline scalp incision and retraction of the skin and temporal muscle. Bleeding was

controlled using a Bovie® cautery. A craniotomy was made over the cerebral cortex with an area of roughly 7 mm^2 (AP: +3.0 to +0.5 mm; ML: ±1 to ±4 mm; relative to bregma [28]) with removal of the overlying meninges. An additional small burr-hole was drilled in a site remote from the recording area for the insertion of a miniature Ag/AgCl reference electrode in the subdural space. The cortical surface was maintained wet with saline soaked cotton balls. An array comprising a CFM-RP-Nafion® and a pulled micropipette (average distance of 75 ± 10 μm) was lowered into the dorsal medial striatum (AP: +1.5–2.0 mm; ML: ±1.5 - ±2.5 mm and DV: −4.0 to −6.0 mm relative to bregma). After insertion of the array into the brain, the baseline was allowed to stabilize for at least 20 min. The mean display frequency was set at 4–20 Hz. An H_2O_2 solution (1 mM in aCSF) was pressure ejected via a Picospritzer II (General Valve, Fairfield, NJ) through a pulled micropipette, with a volume dispensed of 3–125 nL. In experiments in which cardiac arrest was performed during recording session, the rat received a lethal dose of euthanasia solution (0.5 mL of sodium pentobarbital 200 g mL^{-1}, i.p.).

Electrochemical Instrumentation: Electrochemical procedures including RP electrodeposition and CFM evaluation by FCV were performed using a Multi PalmSens4 Potentiostat (PalmSens, The Netherlands) controlled by MultiTrace v.4.2 software (PalmSens, The Netherlands). A 3-electrode electrochemical cell was used, comprised of the working electrode, an Ag/AgCl in 3 M NaCl reference electrode (RE-5B, BAS Inc., IN, USA), and a Pt wire as auxiliary electrode. Amperometric recording in slices and calibration in the slice recording chamber were performed using a FAST16mkII potentiostat (Quanteon, KY, USA) in a 2-electrode electrochemical cell configuration comprised of the working electrode and an Ag/AgCl pellet reference electrode. Amperometric recording *in vivo* in the anesthetized rodent brain was performed using a FAST16mkIII potentiostat (Quanteon, KY, USA) in a 2-electrode electrochemical cell comprised of a working electrode and an Ag/AgCl miniature pseudo reference electrode. The latter was produced by anodization of the exposed tip of the Teflon-coated Ag wire in 1 M HCl saturated with NaCl, which, when in contact with cerebrospinal fluid in the brain containing chloride ions, develops an Ag/AgCl half-cell. Both FAST16 potentiostats were controlled by FAST2014 software (Quanteon, KY, USA). Working potential for monitoring H_2O_2 was set at −0.2 V *vs* Ag/AgCl [25].

Data Analysis. Data analysis was performed using MultiTrace v.4.2, FAST Analysis version 6.0, OriginPro 2016, and GraphPad 5.0. Values are given as the mean ± SEM unless otherwise stated. Normality of data was confirmed using the D'Agostino and Pearson omnibus normality test ($\alpha = 0.05$). Calculated parameters were statistically evaluated by using One-way ANOVA followed by Dunnett post-hoc test. The number of repetitions is indicated in each individual determination. The sensitivity of CFM-RP-Nafion® toward H_2O_2 reduction was determined by linear regression analysis in the range of 0–50 μM. The diffusion of H_2O_2 from a spherical source was modeled using OriginPro 2016, based on equation (1), which describes diffusion from a spherical source [30].

3. Results

3.1. Uptake and removal of extracellular Hydrogen Peroxide in rat brain striatum slices

We evaluated H_2O_2 concentration dynamics in rat striatum slices using previously described CFM-RP-Nafion® sensors [25] in order to investigate how brain tissue handles an increase in extracellular H_2O_2. To this purpose, we constructed an array composed of a H_2O_2 sensor and a null sensor with a tip-to-tip distance of ca. 100 μm. This array was lowered into the tissue core, in the dorsal-medial region of the striatal slice. A micropipette with a tip diameter of 10–20 μm and filled with a 1 mM H_2O_2 solution was placed between the 2 sensors and a volume of solution (25–50 nL) was pressure ejected for a period of 1 s, as depicted in the inset of Fig. 1B. As can be observed in Fig. 1A, repeated H_2O_2 ejections (3 min inter-pulse interval) resulted in transient increases in H_2O_2 in the tissue recorded at the CFM-RP-Nafion® sensor, with no change in the current recorded at the null sensor.

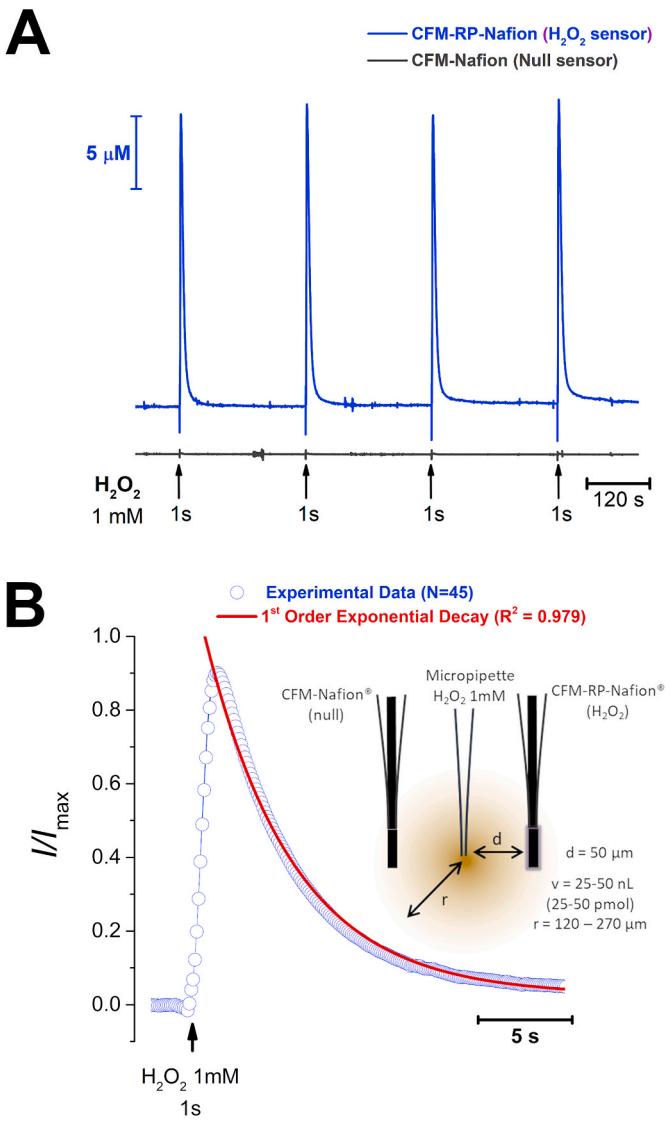

Fig. 1. - A - Recording of H_2O_2 concentration dynamics in striatal slices evoked by exogenous local application of a 1 mM H_2O_2 solution. Blue trace represents the amperometric current measured at the CFM-RP-Nafion® H_2O_2 sensor while the grey trace represents the current recorded at a null sensor. Repeated application of H_2O_2 through a micropipette place between the 2 sensors produced transient and reproducible increase in H_2O_2 in the brain tissue. **B –** Average of 44 individual normalized signals (blue) and first order exponential decay function (red). Inset is a schematic representation of the experimental design used, including the microelectrodes and ejection pipette between the two, where *d* is the distance between the micropipette tip and each of the sensors, *v* is the volume of the H_2O_2 solution ejected from the micropipette and *r* is the calculated radius of the bolus of H_2O_2 ejected. (For interpretation of the references to colour in this figure legend, the reader is referred to the Web version of this article.)

The decay phase of the transient H_2O_2 signal was suitably fitted to a 1st order exponential decay function, shown as the superimposed red line over the experimental data in blue circles in Fig. 1B. From this fitting we determined the time constant of the signal decay, $k = 0.32 \pm 0.02\ s^{-1}$, as well as the decay half-time, $t_{1/2} = 2.5 \pm 0.1$ s (N = 44 signals, obtained from 6 slices).

In order to discriminate the role of brain tissue tortuosity *vs* intracellular processes governing H_2O_2 uptake and breakdown, we repeated

the above experiment in a matrix mimicking tissue tortuosity but devoid of cellular components. We obtained 400 μm slices from a 0.2% agarose block [29,30], which were placed in the slice recording chamber and evaluated H_2O_2 signal obtained as with striatum slices. As summarized in Table 1, the recorded H_2O_2 signals showed slower decay kinetics and the time constant of H_2O_2 decay was significantly decreased as compared to that found in striatal slices ($k = 0.11 \pm 0.01$ s^{-1}) with increase in the signal half-time ($t_{1/2} = 6.5 \pm 0.3$ s, N = 5, $p < 0.0001$). Additionally, we determined the H_2O_2 signal profile in metabolically compromised striatum slices perfused in 0 mM Glucose, 10 mM Saccharose and 10 mM CN^-. Under these conditions, the H_2O_2 signal was similar to that observed in agarose slices and the decay time constant ($k = 0.12 \pm 0.01$ s^{-1}) and signal half-time ($t_{1/2} = 5.8 \pm 0.5$ s) were significantly changed as compared to control tissue ($p < 0.0001$). These results support a role for cellular components in shaping extracellular H_2O_2 concentration dynamics.

3.2. Hydrogen Peroxide removal In Vivo in the rat striatum

Slice preparations preserve tissue cytoarchitecture and allow us to understand the role of neural cells (neurons and astrocytes) in modulating the concentration dynamics of diffusible species such as H_2O_2. However, they are devoid of functional vasculature. Hence, we investigated H_2O_2 signal profiles *in vivo* in the striatum of anesthetized rats. Similar to what was previously observed in striatal slices, local pressure ejection of a 1 mM solution resulted in a transient increase in H_2O_2 recorded at the CFM-RP-Nafion® H_2O_2 sensor inserted in the dorsal medial striatum *in vivo* in the anesthetized rat brain and repetitive ejections produced reproducible signals *in vivo* (Fig. S1).

The decay phase of the signal was well adjusted to a 1st order exponential decay function (Fig. 2A) and average time constant was determined to be $k = 0.34 \pm 0.01$ s^{-1}, corresponding to an average $t_{1/2} = 2.2 \pm 0.1$ s (N = 121 signals, obtained from 12 recording sessions, Table 1), similar to that observed in slices. Furthermore, the average peak concentration of H_2O_2 measured at the detector was 30.5 ± 2.5 μM. We repeated this paradigm using a higher concentration of H_2O_2 (10 mM) and observed that the average time constant significantly decreased to $k = 0.20 \pm 0.02$ s^{-1} (N = 43 signals, obtained from 3 recording sessions, Table 1) and the average H_2O_2 peak concentration was increased to 105.9 ± 30.4 μM. This result suggests that for 10 mM H_2O_2, the Prx pool becomes partially hyperoxidized [31], which might hinder its participation in H_2O_2 removal, resulting in slower H_2O_2 clearance by the tissue. For the remainder of the experiments we used a 1 mM H_2O_2 solution.

Induction of cardiac arrest resulted in rapid loss of spontaneous brain wave activity accompanied by a gradual decrease of the k values (Fig. 2B). As summarized in Table 1, the average time constant value stabilized at $k = 0.21 \pm 0.03$ (N = 19), a value significantly lower when compared to the control situation, but similar to that observed in slices following metabolic poisoning ($p = 0.87$) and in a 0.2% agarose block ($p = 0.83$) used as a mimetic of brain tissue tortuosity. The onset of decrease in k values coincided with the decrease in power observed in the spectrogram, known to reflect brain wave activity [32–34].

Table 1
Comparison of decay time constant (k) and half-life ($t_{1/2}$) of H_2O_2 signals obtained in response to puff ejections of a 1 mM H_2O_2 solution, unless otherwise indicated. Data were obtained in *ex vivo* acute striatal slices and 0.2% agarose slices, and *in vivo* in the dorsal medial striatum in anesthetized rat and in a 0.2% agarose block at 37 °C. Values represent mean ± SEM. *$p < 0.0001$ as compared to control slices and #$p < 0.001$ as compared to *in vivo* control (1 mM H_2O_2).

Experimental Model (N)		k / s^{-1}	$t_{1/2}$ / s
Ex vivo - Striatum Slices	Control (44)	0.32 ± 0.02	2.5 ± 0.1
	MC (5)	0.12 ± 0.01*	5.8 ± 0.5*
	Agarose 0.2% (5)	0.11 ± 0.01*	6.5 ± 0.3*
In vivo - Dorsal Medial Striatum	Control (121)	0.34 ± 0.01	2.2 ± 0.1
	10 mM H_2O_2 (42)	0.23 ± 0.02#	3.5 ± 0.2#
	A.D. (19)	0.21 ± 0.03#	4.8 ± 0.7#
	Agarose 0.2% (26)	0.04 ± 0.004#	18.6 ± 1.2#

MC – metabolically compromised slices, perfused with 0 mM glucose, 10 mM saccharose and 10 mM CN^-.
A.D. – after death evoked by lethal dose of pentobarbital.

3.3. Estimation of Hydrogen Peroxide diffusion coefficient in vivo in the striatum

In order to determine de *in vivo* effective diffusion coefficient (D^*) of exogenously applied H_2O_2 in striatum tissue, the experimental data were input to Eq. (1) where C and C_0 represent the instantaneous and initial concentration, r is the radius of the sphere of H_2O_2 ejected, d is the distance between source (pipette) and recorder (H_2O_2 sensor), t is time, D^* the effective diffusion coefficient and λ represents the inactivation constant.

$$C = C_0\, e^{-\lambda t}\left[\frac{1}{2}\left(erf\left(\frac{r+d}{2\sqrt{D^* t}}\right) - erf\left(\frac{r-d}{2\sqrt{D^* t}}\right)\right) - \frac{1}{d}\cdot\sqrt{\frac{D^* t}{\pi}}\left(e^{\frac{-(r-d)^2}{4 D^* t}} - e^{\frac{-(r+d)^2}{4 D^* t}}\right)\right] \quad (1)$$

The experimental design was adjusted to guarantee $r < d$, as illustrated in Fig. 3B. Recordings were obtained both *in vivo*, in the striatum of anesthetized rats and from a 0.2% agarose gel block at 37 °C. As shown in Fig. 3A, in both cases we observed a good adjustment between the experimental data (open circles) and the fit to Eq. (1) (line).

We determined the $D^*_{in\ vivo}$ of H_2O_2 to be $(2.5 \pm 0.1) \times 10^{-5}$ cm^2 s^{-1} with an average inactivation constant of $\lambda = 0.19 \pm 0.01$ s^{-1} (N = 57 obtained from 5 recording sessions). Interestingly, this value of D^* was found to be significantly higher than that calculated from data obtained in agarose gel, where we observe $D^*_{agarose} = (1.7 \pm 0.1 \times 10^{-5})$ cm^2 s^{-1} and an inactivation constant of $\lambda = 0.005 \pm 0.002$ s^{-1} (N = 38).

From the Einstein-Smoluchowski Eq. (2) one can define the average square of the distance travelled ($\overline{x^2}$) by an individual molecule as a function D and t [35]. As can be appreciated in Fig. 4, H_2O_2 can be classified in the same range as small volume neurotransmitters such as nitric oxide ($^{\bullet}NO$), displaying a relatively large displacement within its $t_{1/2}$ (112 μm) when compared to other neurotransmitters such as dopamine or glutamate (properties summarized in Table 2).

$$\overline{x^2} = 2Dt \quad (2)$$

4. Discussion

Interest in monitoring H_2O_2 in brain tissue extracellular space has grown over the past years as a result of increasing recognition of its involvement not only in the etiology of neurodegenerative disorders such as Parkinson's and Alzheimer's diseases [39], but also due to the appreciation of its putative role as a diffusible neuromodulator, analogous to $^{\bullet}NO$ [5,40]. Recent advances in the identification of membrane H_2O_2 transporters, beyond the passive diffusion through membranes, support that the extracellular H_2O_2 dynamics might modulate intracellular redox signaling pathways in cells localized within the volume of influence of H_2O_2. Here, we have investigated the extracellular concentration dynamics of H_2O_2 in the striatum, a brain region where H_2O_2 has been proposed to act as an intercellular messenger molecule, modulating dopamine release from midbrain afferent fibers [41,42], focusing on determining H_2O_2 half-life time in brain tissue in an *ex vivo* model (striatal slices) and *in vivo* in the striatum of anesthetized rats. In addition, we have determined the effective diffusion coefficient of H_2O_2 in brain tissue *in vivo*. We used an artificial peroxidase type electrochemical microsensor [25] to monitor real-time H_2O_2 concentration dynamics in the brain extracellular space with high sensitivity and selectivity towards H_2O_2 and high spatial and temporal resolution

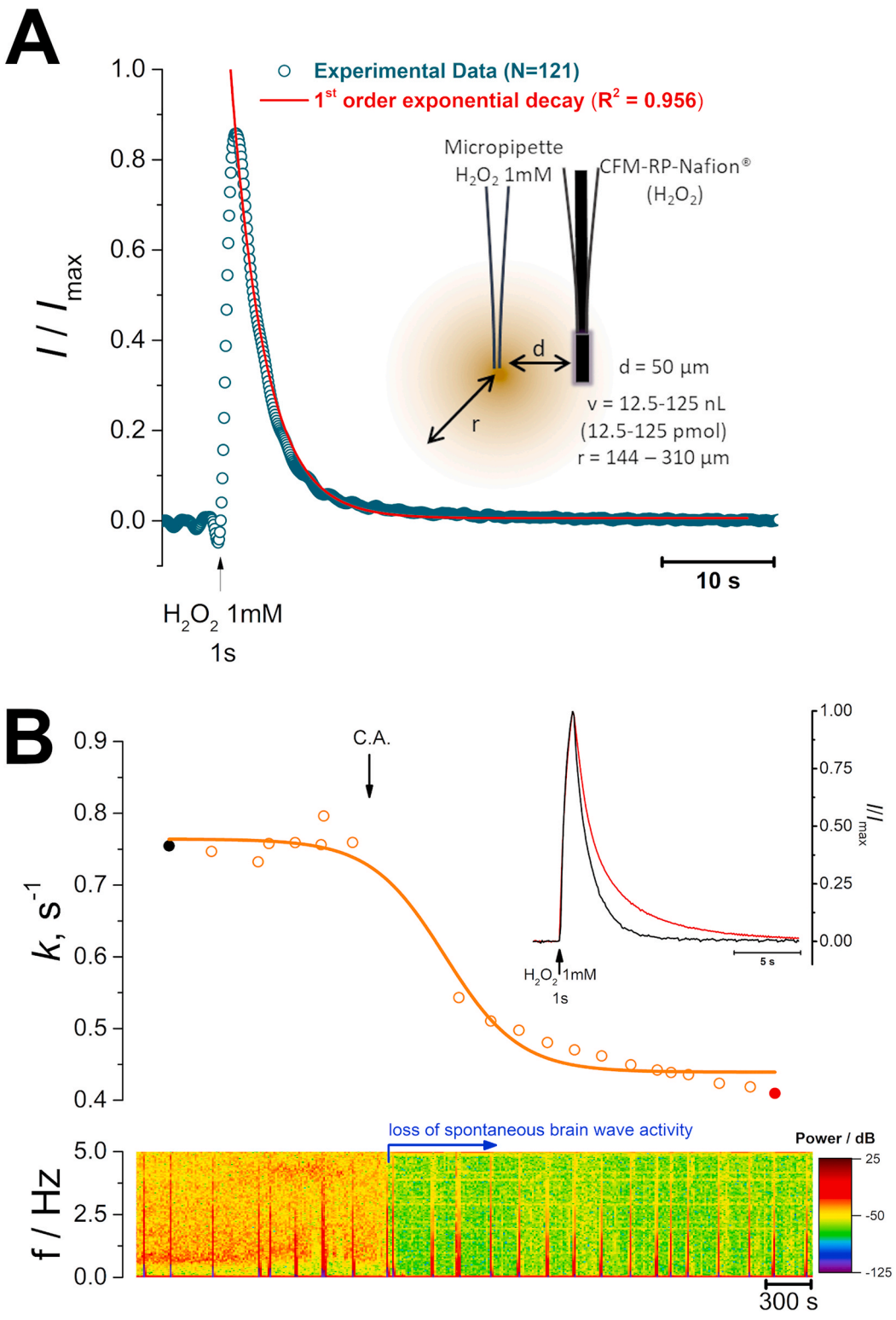

Fig. 2. – A - Recording of H_2O_2 concentration dynamics *in vivo* in the dorsal medial striatum (AP: +1.8, ML: −2.0; DV: −4.5 mm) evoked by exogenous local application of a H_2O_2 1 mM solution. Fitting of experimental data to a 1st order decay function (red line). Inset is a schematic representation of the experimental design used, including the microelectrodes and ejection pipette between the two, where *d* is the distance between the micropipette tip and the CFM-RP-Nafion® sensor, *v* is the volume of the H_2O_2 solution ejected from the micropipette and *r* is the calculated radius of the bolus of H_2O_2 ejected. **B** – Representative trace of the observed change in time constant value before and after induction of cardiac arrest as a function of time (top). Inset are superimposed the first (black) and last (red) signals. On the bottom is the power spectrum of the 10 Hz amperometric recording, showing the marked loss in power following cardiac arrest, indicative of loss of spontaneous brain wave activity. (For interpretation of the references to colour in this figure legend, the reader is referred to the Web version of this article.)

resulting from the reduced sensor size (o.d. 33 µm) and the fast-sampling ability of amperometry. In both experimental models, we coupled a micropipette to the microsensor to apply a controlled pressure ejection of a nL volume of a H_2O_2 solution at a known distance from the detector. Through mathematical fitting of the data, to the best of our knowledge, we provide the first *in vivo* data regarding the effective or apparent diffusion coefficient of H_2O_2 in the living brain.

Hydrogen Peroxide is Rapidly Removed from the Extracellular Space by Metabolically Active Cells. In the first set of experiments, we investigated the extracellular concentration dynamics of H_2O_2 in an *ex vivo* model of acute striatum slices. This experimental model has the advantage of preserving the brain tissue cytoarchitectural integrity, namely connectivity and intercellular communication. Because cerebrovascular blood flow is absent in this model, it allows us to better understand the role of neural cells (astrocytes and neurons) without the contribution of blood flow. Our data revealed that a puff application of a

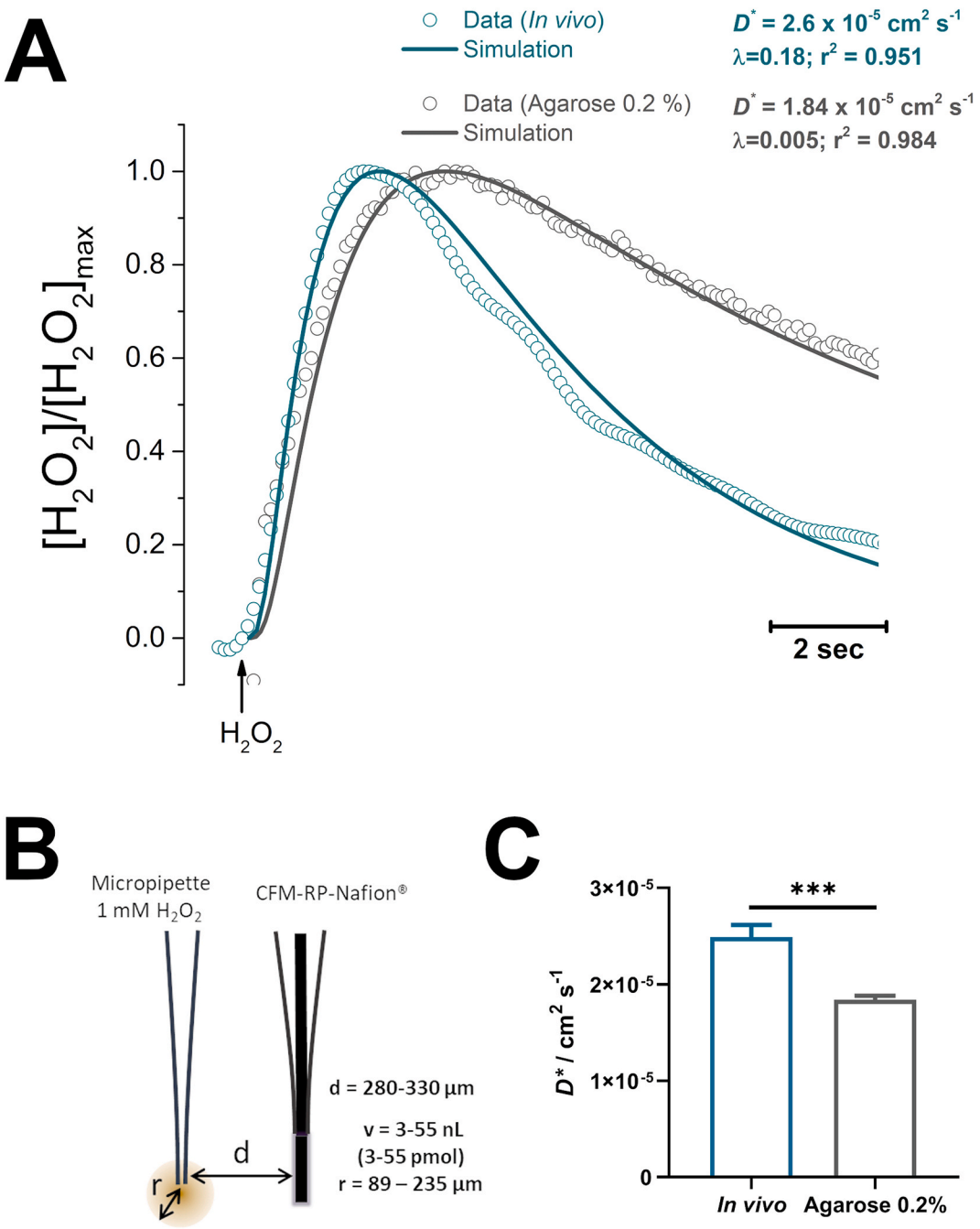

Fig. 3. **– A -** Representative recordings of H_2O_2 concentration dynamics obtained *in vivo* in the striatum (blue-green) and in a 0.2% agarose block at 37 °C (grey). Circles represent experimental data while lines correspond to the theoretical trace obtained by modelling expression (1). **B** – Experimental design used, comprising a micropipette filled with a 1 mM H_2O_2 solution coupled to a CFM-RP-Nafion® sensor for H_2O_2 detection. Interval of distance (d) between source and detector as well as for the volume and radius of applied H_2O_2 bolus are discriminated. As drawn, d = 300 µm and r = 100 µm. **C** – Effective diffusion coefficient values calculated by modelling experimental data with Eq. (1). (For interpretation of the references to colour in this figure legend, the reader is referred to the Web version of this article.)

H_2O_2 solution in the proximity of the detector resulted in a transient increase in H_2O_2 concentration, revealing that extracellular H_2O_2 diffuses away from the point of origin and is rapidly removed. Removal of exogenously applied H_2O_2 was found to be the result of intracellular factors, as the decay was significantly slower in a 0.2% agarose slice. Agarose has been widely used to mimic brain tissue tortuosity and to evaluate its effect on the diffusion of chemical species [29,30]. In line with this observation, in metabolically compromised striatal slices perfused with CN^- and 0 mM glucose as a strategy to hinder energy metabolism, H_2O_2 decay was found to be similar to that observed in agarose. Taken together, these results support the notion that extracellular H_2O_2 enters cells, namely neurons and/or astrocytes, and is removed in metabolically competent cells, presumably through the activity of enzymatic systems such as GPx, Prx and CAT.

Similarly, *in vivo,* we also observed that puff application of an H_2O_2 solution resulted in a transient increase in extracellular H_2O_2, with a decay rate superior to that found in a 0.2% agarose block. Following cardiac arrest, the decay rate of the signal decreased progressively, but remained above that found in agarose. We speculate that this is the result of H_2O_2 removal by erythrocytes, namely due to the activity of catalase which does not consume redox equivalents when degrading H_2O_2 [43]. While in neurons and astrocytes, catalase is mainly found in

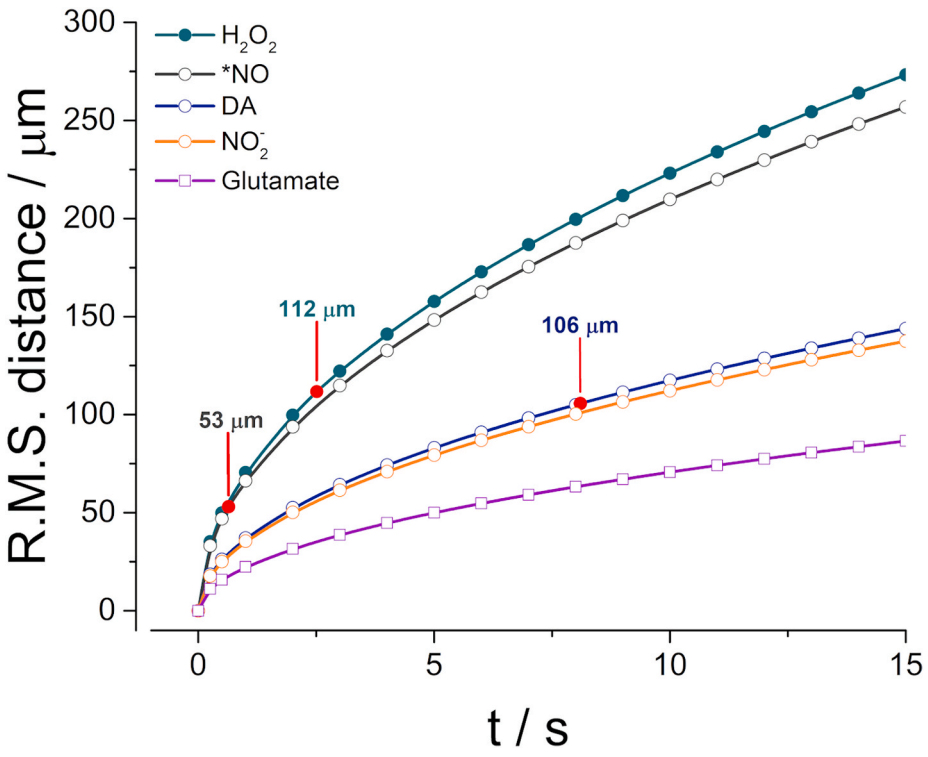

Fig. 4. Calculated root-mean-square (R.M.S.) distance of random movement for H_2O_2 using Eq. (2) and considering D^* values calculated in present study. For comparative purposes we have also plotted data for •NO (grey), dopamine (DA, blue), NO_2^- (orange) and glutamate (purple). Red circles represent distance travelled by each analyte for their respective extracellular half-life time ($t_{1/2}$). (For interpretation of the references to colour in this figure legend, the reader is referred to the Web version of this article.)

Table 2
Comparative analysis of half-life and apparent diffusion coefficient for H_2O_2 and other species acting as volume transmission molecules (•NO and dopamine) as well as the fast-excitatory neurotransmitter glutamate. Nitrite has been included to show the effect of charge on a small molecule.

Analyte	Experimental Model	$t_{1/2}$ (s)	D^* (x 10^{-5} cm^2 s^{-1})	Ref
H_2O_2	*In vivo* in the rat striatum	2.2	2.5	Present Study
•NO	*In vivo* in the rat cortex	0.6	3.3	[36]
Dopamine	Midbrain slices from Guinea pig	8.1	0.69	[37]
Nitrite	*In vivo* in the rat cortex	n.d.	0.63	[36]
Glutamate	Mathematical Modelling	n.d.	0.25	[38]

peroxisomes and thus less accessible to exogenously derived H_2O_2, erythrocytes do not have membrane organelles and CAT is found in the cytosol. Even after cardiac arrest, erythrocytes present in blood vessels may, temporarily, contribute to H_2O_2 removal in brain tissue.

Half-Life of Hydrogen Peroxide in the Brain Extracellular Space: The average half-life of extracellular H_2O_2 in slices and *in vivo* were 2.5 and 2.2 s respectively, values that are not statistically different from each other. Neuromodulators such as •NO have been shown to have a half-life time of 0.42 and 0.75 s in cortex and hippocampus, respectively [44] while dopamine is reported to have $t_{1/2}$ values ranging from 7.4 to 8.1 s [37]. The removal of each one of the messengers is governed by different biochemical and cellular pathways. •NO inactivation is tightly coupled to its facile reaction with hemoglobin in circulating erythrocytes [44,45]. •NO produced in response to glutamatergic neurotransmission evokes vasodilation, increasing local blood flow and the concentration of hemoglobin [46,47]. Additionally, •NO does not require transporters to cross biomembranes: due to its hydrophobic nature, the free radical readily crosses phospholipid bilayers or uses them as fast diffusion highways [36,48]. Dopamine clearance from the extracellular space depends on the activity of the neuronal dopamine transporter (DAT), a member of the neurotransmitter sodium symporter protein superfamily (reviewed in Ref. [49]). While H_2O_2 can, to a limited extent, cross biomembranes by simple diffusion, it is currently accepted that it can gain rapid entry into the cells through water channels – aquaporins (AQP). These are membrane channels that facilitate the passage of water and other non-charged solutes across biological membranes down their concentration gradients [50]. Within the group of channels, those that display permeability for H_2O_2 (AQP3, AQP8 and AQP9) have been coined peroxiporins [51–53]. Considering the large concentration gradient existing between extra- and intracellular compartments, one can expect any increase in extracellular H_2O_2 to rapidly enter the cell, where it is rapidly decomposed by GPx, Prx or CAT. The existence of peroxiporins helps to understand the smaller $t_{1/2}$ of H_2O_2 as compared to dopamine, for example.

Effective Diffusion Coefficient and Inactivation Constant of Hydrogen Peroxide in Brain Tissue: To operate as an intercellular signaling molecule, H_2O_2 must diffuse in the extracellular space. We have previously investigated the diffusion of •NO in brain tissue, using both experimental-based and mathematical modelling strategies to better understand its concentration dynamics in the brain [36,44,54]. We adjusted data obtained in a 0.2% agarose block and *in vivo* using a previously described mathematical model for diffusion of a chemical species from a spherical source (equation (1) [55]) to determine and compare the effective diffusion coefficient of H_2O_2 (D^*) and its inactivation constant (λ). Data obtained in agarose revealed an average diffusion coefficient of 1.7×10^{-5} cm^2 s^{-1}, in line with that reported for aqueous buffer of 1.8×10^{-5} cm^2 s^{-1} [56]. Additionally, the fact that the inactivation constant in agarose is close to zero ($\lambda = 0.005$) corroborated that inactivation mechanisms did not contribute to shaping of H_2O_2 diffusion in agarose, as expected. Modeling data obtained *in vivo* revealed a λ value of $\lambda = 0.19$ s^{-1}, which is a range similar to the decay constant calculated from the exponential fit of data from slices and *in vivo* (ca. 0.3 s^{-1}), implying that inactivation plays an important role in shaping extracellular concentration dynamics.

We found the *in vivo* effective diffusion coefficient of H_2O_2 to be slightly higher than that observed in agarose, assuming and average value of $D^* = 2.5 \times 10^{-5}$ cm^2 s^{-1}. This is a curious observation, as one would expect to observe hindrance of diffusion in the extracellular space

as compared to free diffusion in buffer (reported to be $D = 1.8 \times 10^{-5}$ cm^2 s^{-1} at 37 °C [56]).

Hydrogen Peroxide is a Volume Transmission Signaling Molecule: From Eq. (2) we can observe that the mean distance a single molecule of H_2O_2 can travel *in vivo* in the brain is similar to that we have previously described for the highly diffusible intercellular messenger $^{\bullet}NO$ [36] and much higher than what is expected for neuromodulators such as dopamine or a fast synaptic neurotransmitter such as glutamate. Interestingly, because the inactivation constant for H_2O_2 is lower than that for $^{\bullet}NO$, which is rapidly removed by rapid reaction with oxyhemoglobin ($k = 3.4 \times 10^7$ M^{-1} s^{-1} [57]), H_2O_2 may in fact diffuse larger distances in the brain tissue.

Considering this, we can tentatively place H_2O_2 within the class of volume transmitters in the brain, of which $^{\bullet}NO$ is a paradigmatic example. Volume transmission is a form of intercellular communication in which the signaling molecule diffuses in the extracellular space, connecting all cell types in the brain, in what Agnati and Fuxe have coined "complex cellular networks" [58,59]. The diffusion or migration of the signal is terminated when the signaling molecule is removed by enzymes, cleared by brain capillaries or taken up by transporters. In support of this notion, several cell studies support the role of H_2O_2 as a neuromodulator in the brain. Micromolar levels of H_2O_2 (1–50 μM) have been shown to modulate synaptic plasticity by inducing the release of Ca^{2+} from intracellular stores which can then activate a myriad of Ca^{2+}-dependent proteins and alter neuronal Ca^{2+} permeability [3]. Additionally, H_2O_2 has been shown to be important in modulating dopamine release in the striatum in a signaling pathway that includes glutamate-evoked H_2O_2 production (presumably in mitochondria) and diffusion from medium spiny neurons to modulate dopamine release from midbrain axons via opening of K_{ATP} channels [41,42,60]. The present works consolidates these findings, providing quantitative and direct bases on how extracellular H_2O_2 diffuses in the extracellular space and highlighting the major contributors towards shaping its concentration dynamics *in vivo*.

5. Conclusions

Hydrogen peroxide has been established as a ubiquitous redox signaling molecule in a new paradigm of cell communication. However, a fine line separates oxidative eustress (physiological signaling) from and oxidative distress (disease processes). In the present work, using a novel sensing strategy based on an artificial-peroxidase amperometric microsensor, we have investigated the quantitative determinants of the extracellular concentration dynamics of H_2O_2 in the brain tissue. Our data reveal the *in vivo* effective diffusion coefficient and half-life of H_2O_2, supporting a role as a volume signaling molecule in the striatum. The concept of the emerging field of redox medicine, which aims to apply redox modulation as a therapeutic strategy requires that we first comprehend signaling pathways by combining experimental data with mathematical modeling to deconstruct signals associated with specific redox molecules and determine their spatial and temporal pattern of change in tissue.

Author contributions

AL – Corresponding author; Experiment design and conception; Experiment performance; Data Analysis; Writing of manuscript.

EF – Microelectrode construction and evaluation; data analysis.

AS – Writing and critical revision of manuscript.

JL – Experimental design; critical revision of manuscript.

RB – Experiment design and conception; data analysis; critical revision of manuscript; funding.

Declaration of competing interest

The authors declare no conflict of interests.

Acknowledgements

This work was financed by the European Regional Development Fund (ERDF) through the COMPETE 2020 – Operational Programme for Competitiveness and Internationalization, and by Portuguese national Funds via FCT – Fundação para a Ciência e Tecnologia, under projects POCI-01-0145-FEDER-028261, POCI-01-0145-FEDER-029099 and UIDB/04539/2020.

Appendix A. Supplementary data

Supplementary data to this article can be found online at https://doi.org/10.1016/j.redox.2022.102250.

References

[1] H. Sies, D.P. Jones, Reactive oxygen species (ROS) as pleiotropic physiological signalling agents, Nat. Rev. Mol. Cell Biol. (2020) 1–21, https://doi.org/10.1038/s41580-020-0230-3.

[2] M.C.W. Oswald, N. Garnham, S.T. Sweeney, M. Landgraf, Regulation of neuronal development and function by ROS, FEBS Lett 592 (2018) 679–691, https://doi.org/10.1002/1873-3468.12972.

[3] A. Kamsler, M. Segal, Hydrogen peroxide as a diffusible signal molecule in synaptic plasticity, Mol. Neurobiol. 29 (2004) 167–178, https://doi.org/10.1385/MN:29:2:16, 7.

[4] D.S.A. Simpson, P.L. Oliver, ROS generation in microglia: understanding oxidative stress and inflammation in neurodegenerative disease, Antioxidants 9 (2020) 743, https://doi.org/10.3390/antiox9080743.

[5] J.C. Patel, M.E. Rice, Classification of H 2 O 2 as a neuromodulator that regulates striatal dopamine release on a subsecond time scale, ACS Chem. Neurosci. 3 (2012) 991–1001, https://doi.org/10.1021/cn300130b.

[6] O. Lyublinskaya, F. Antunes, Measuring intracellular concentration of hydrogen peroxide with the use of genetically encoded H2O2 biosensor HyPer, Redox Biol 24 (2019) 101200, https://doi.org/10.1016/j.redox.2019.101200.

[7] B. Chance, H. Sies, A. Boveris, Hydroperoxide metabolism in mammalian organs, Physiol. Rev. 59 (1979) 527–605, https://doi.org/10.1152/physrev.1979.59.3.527.

[8] H.J. Forman, A. Bernardo, K.J.A. Davies, What is the concentration of hydrogen peroxide in blood and plasma? Arch. Biochem. Biophys. 603 (2016) 48–53, https://doi.org/10.1016/j.abb.2016.05.005.

[9] R. Benfeitas, G. Selvaggio, F. Antunes, P.M.B.M. Coelho, A. Salvador, Hydrogen peroxide metabolism and sensing in human erythrocytes: a validated kinetic model and reappraisal of the role of peroxiredoxin II, Free Radic. Biol. Med. 74 (2014) 35–49, https://doi.org/10.1016/j.freeradbiomed.2014.06.007.

[10] B. Frei, Y. Yamamoto, D. Niclas, B.N. Ames, Evaluation of an isoluminol chemiluminescence assay for the detection of hydroperoxides in human blood plasma, Anal. Biochem. 175 (1988) 120–130, https://doi.org/10.1016/0003-2697(88)90369-7.

[11] A. Nahum, L.D.H. Wood, J. Iasha Sznajder, Measurement of hydrogen peroxide in plasma and blood, Free Radic. Biol. Med. 6 (1989) 479–484, https://doi.org/10.1016/0891-5849(89)90040-3.

[12] C. Gao, Y. Tian, R. Zhang, J. Jing, X. Zhang, Endoplasmic reticulum-directed ratiometric fluorescent probe for quantitive detection of basal H2O2, Anal. Chem. 89 (2017) 12945–12950, https://doi.org/10.1021/acs.analchem.7b03809.

[13] J.B. Lim, B.K. Huang, W.M. Deen, H.D. Sikes, Analysis of the lifetime and spatial localization of hydrogen peroxide generated in the cytosol using a reduced kinetic model, Free Radic. Biol. Med. 89 (2015) 47–53, https://doi.org/10.1016/j.freeradbiomed.2015.07.009.

[14] R.D.M. Travasso, F. Sampaio dos Aidos, A. Bayani, P. Abranches, A. Salvador, Localized redox relays as a privileged mode of cytoplasmic hydrogen peroxide signaling, Redox Biol 12 (2017) 233–245, https://doi.org/10.1016/j.redox.2017.01.003.

[15] F. Orrico, A.C. Lopez, D. Saliwonczyk, C. Acosta, I. Rodriguez-Grecco, I. Mouro-Chanteloup, M.A. Ostuni, A. Denicola, L. Thomson, M.N. Möller, The permeability of human red blood cell membranes to hydrogen peroxide is independent of aquaporins, J. Biol. Chem. 298 (2022) 101503, https://doi.org/10.1016/j.jbc.2021.101503.

[16] A.C. Matias, N. Pedroso, N. Teodoro, H.S. Marinho, F. Antunes, J.M. Nogueira, E. Herrero, L. Cyrne, Down-regulation of fatty acid synthase increases the resistance of Saccharomyces cerevisiae cells to H2O2, Free Radic. Biol. Med. 43 (2007) 1458–1465, https://doi.org/10.1016/J.FREERADBIOMED.2007.08.003.

[17] F. Antunes, E. Cadenas, Estimation of H2O2 gradients across biomembranes, FEBS Lett 475 (2000) 121–126, https://doi.org/10.1016/S0014-5793(00)01638-0.

[18] G.P. Bienert, F. Chaumont, Aquaporin-facilitated transmembrane diffusion of hydrogen peroxide, Biochim. Biophys. Acta Gen. Subj. 1840 (2014) 1596–1604, https://doi.org/10.1016/j.bbagen.2013.09.017.

[19] C.C. Winterbourn, Biological production, detection, and fate of hydrogen peroxide, Antioxidants Redox Signal. 29 (2018) 541–551, https://doi.org/10.1089/ars.2017.7425.

[20] S. Stöcker, K. Van Laer, A. Mijuskovic, T.P. Dick, The conundrum of hydrogen peroxide signaling and the emerging role of peroxiredoxins as redox relay hubs,

Antioxidants Redox Signal. 28 (2018) 558–573, https://doi.org/10.1089/ars.2017.7162.
[21] H.N. Kirkman, G.F. Gaetani, Mammalian catalase: a venerable enzyme with new mysteries, Trends Biochem. Sci. 32 (2007) 44–50, https://doi.org/10.1016/j.tibs.2006.11.003.
[22] H.N. Kirkman, S. Galiano, G.F. Gaetani, The function of catalase-bound NADPH, J. Biol. Chem. 262 (1987) 660–666, https://doi.org/10.1016/s0021-9258(19)75835-9.
[23] C.C. Winterbourn, A.J. Kettle, M.B. Hampton, Reactive oxygen species and neutrophil function, Annu. Rev. Biochem. 85 (2016) 765–792, https://doi.org/10.1146/annurev-biochem-060815-014442.
[24] E. Syková, C. Nicholson, Diffusion in brain extracellular space, Physiol. Rev. 88 (2008) 1277–1340, https://doi.org/10.1152/physrev.00027.2007.
[25] A. Ledo, E. Fernandes, C.M.A. Brett, R.M. Barbosa, Enhanced selectivity and stability of ruthenium purple-modified carbon fiber microelectrodes for detection of hydrogen peroxide in brain tissue, Sensor. Actuator. B Chem. 311 (2020) 127899, https://doi.org/10.1016/j.snb.2020.127899.
[26] R.M. Santos, C.F. Lourenço, A.P. Piedade, R. Andrews, F. Pomerleau, P. Huettl, G. A. Gerhardt, J. Laranjinha, R.M. Barbosa, A comparative study of carbon fiber-based microelectrodes for the measurement of nitric oxide in brain tissue, Biosens. Bioelectron. 24 (2008) 704–709, https://doi.org/10.1016/j.bios.2008.06.034.
[27] R.M. Barbosa, C.F. Lourenço, R.M. Santos, F. Pomerleau, P. Huettl, G.A. Gerhardt, J. Laranjinha, In vivo real-time measurement of nitric oxide in anesthetized rat brain, in: Methods Enzymol., 2008, pp. 351–367, https://doi.org/10.1016/S0076-6879(08)01220-2.
[28] G. Paxinos, Charles Watson, The Rat Brain in Stereotaxic Coordinates, sixth ed., 2007.
[29] R. Pomfret, G. Miranpuri, K. Sillay, The substitute brain and the potential of the gel model, Ann. Neurosci. 20 (2013) 118–122, https://doi.org/10.5214/ans.0972.7531.200309.
[30] R. Pomfret, K. Sillay, G. Miranpuri, Investigation of the electrical properties of Agarose Gel: characterization of concentration using nyquist plot phase angle and the implications of a more comprehensive in vitro model of the Brain, Ann. Neurosci. 20 (2013) 99–107, https://doi.org/10.5214/ans.0972.7531.200305.
[31] Z.A. Wood, L.B. Poole, P.A. Karplus, Peroxiredoxin evolution and the regulation of hydrogen peroxide signaling, 80, Science 300 (2003) 650–653, https://doi.org/10.1126/science.1080405.
[32] A. Ledo, C.F. Lourenço, J. Laranjinha, G.A. Gerhardt, R.M. Barbosa, Concurrent measurements of neurochemical and electrophysiological activity with microelectrode arrays: new perspectives for constant potential amperometry, Curr. Opin. Electrochem. 12 (2018) 129–140, https://doi.org/10.1016/j.coelec.2018.05.018.
[33] A. Ledo, C.F. Lourenço, J. Laranjinha, G.A. Gerhardt, R.M. Barbosa, Combined in vivo amperometric oximetry and electrophysiology in a single sensor: a tool for Epilepsy research, Anal. Chem. 89 (2017) 12383–12390, https://doi.org/10.1021/acs.analchem.7b03452.
[34] C.F.C.F. Lourenço, A. Ledo, G.A.G.A. Gerhardt, J. Laranjinha, R.M.R.M. Barbosa, Neurometabolic and electrophysiological changes during cortical spreading depolarization: multimodal approach based on a lactate-glucose dual microbiosensor arrays, Sci. Rep. 7 (2017) 1–12, https://doi.org/10.1038/s41598-017-07119-6.
[35] M.A. Islam, Einstein–smoluchowski diffusion equation: a discussion, Phys. Scripta 70 (2004) 120–125, https://doi.org/10.1088/0031-8949/70/2-3/008.
[36] R.M. Santos, C.F. Lourenço, G.A. Gerhardt, E. Cadenas, J. Laranjinha, R. M. Barbosa, Evidence for a pathway that facilitates nitric oxide diffusion in the brain, Neurochem. Int. 59 (2011) 90–96, https://doi.org/10.1016/j.neuint.2011.05.016.
[37] S.J. Cragg, C. Nicholson, J. Kume-Kick, L. Tao, M.E. Rice, Dopamine-mediated volume transmission in midbrain is regulated by distinct extracellular geometry and uptake, J. Neurophysiol. 85 (2001) 1761–1771, https://doi.org/10.1152/jn.2001.85.4.1761.
[38] W.R. Holmes, Modeling the effect of glutamate diffusion and uptake on NMDA and non-NMDA receptor saturation, Biophys. J. 69 (1995) 1734–1747, https://doi.org/10.1016/S0006-3495(95)80043-3.
[39] M. Jimenez Del Rio, C. Velez-Pardo, The hydrogen peroxide and its importance in Alzheimers and Parkinsons disease, Curr. Med. Chem. Nerv. Syst. Agents. 4 (2004) 279–285, https://doi.org/10.2174/1568015043356896.
[40] C.R. Lee, J.C. Patel, B. O'Neill, M.E. Rice, Inhibitory and excitatory neuromodulation by hydrogen peroxide: translating energetics to information, J. Physiol. 593 (2015) 3431–3446, https://doi.org/10.1113/jphysiol.2014.273839.
[41] J.C. Patel, P. Witkovsky, W.A. Coetzee, M.E. Rice, Subsecond regulation of striatal dopamine release by pre-synaptic KATP channels, J. Neurochem. 118 (2011) 721–736, https://doi.org/10.1111/j.1471-4159.2011.07358.x.
[42] L. Bao, M.V. Avshalumov, J.C. Patel, C.R. Lee, E.W. Miller, C.J. Chang, M.E. Rice, Mitochondria are the source of hydrogen peroxide for dynamic brain-cell signaling, J. Neurosci. 29 (2009) 9002–9010, https://doi.org/10.1523/JNEUROSCI.1706-09.2009.
[43] H.N. Kirkman, G.F. Gaetani, Mammalian catalase: a venerable enzyme with new mysteries, Trends Biochem. Sci. 32 (2007) 44–50, https://doi.org/10.1016/j.tibs.2006.11.003.
[44] R.M. Santos, C.F. Lourenço, F. Pomerleau, P. Huettl, G.A. Gerhardt, J. Laranjinha, R.M. Barbosa, Brain nitric oxide inactivation is governed by the vasculature, Antioxidants Redox Signal. 14 (2011) 1011–1021, https://doi.org/10.1089/ars.2010.3297.
[45] I. Azarov, K.T. Huang, S. Basu, M.T. Gladwin, N. Hogg, D.B. Kim-Shapiro, Nitric oxide scavenging by red blood cells as a function of hematocrit and oxygenation, J. Biol. Chem. 280 (2005) 39024–39032, https://doi.org/10.1074/jbc.M509045200.
[46] A. Ledo, C.F. Lourenço, E. Cadenas, R.M. Barbosa, J. Laranjinha, The bioactivity of neuronal-derived nitric oxide in aging and neurodegeneration: switching signaling to degeneration, Free Radic. Biol. Med. 162 (2021) 500–513, https://doi.org/10.1016/j.freeradbiomed.2020.11.005.
[47] C.F. Lourenço, R.M. Santos, R.M. Barbosa, E. Cadenas, R. Radi, J. Laranjinha, Neurovascular coupling in hippocampus is mediated via diffusion by neuronal-derived nitric oxide, Free Radic. Biol. Med. 73 (2014) 421–429, https://doi.org/10.1016/j.freeradbiomed.2014.05.021.
[48] M.N. Möller, A. Denicola, Diffusion of nitric oxide and oxygen in lipoproteins and membranes studied by pyrene fluorescence quenching, Free Radic. Biol. Med. 128 (2018) 137–143, https://doi.org/10.1016/j.freeradbiomed.2018.04.553.
[49] K.C. Schmitt, M.E.A. Reith, Regulation of the dopamine transporter: aspects relevant to psychostimulant drugs of abuse, Ann. N. Y. Acad. Sci. 1187 (2010) 316–340, https://doi.org/10.1111/j.1749-6632.2009.05148.x.
[50] R.N. Finn, J. Cerdà, Evolution and functional diversity of aquaporins, Biol. Bull. 229 (2015) 6–23, https://doi.org/10.1086/BBLv229n1p6.
[51] S. Watanabe, C. Sagita Moniaga, S. Nielsen, M. Hara-Chikuma, C.S. Moniaga, S. Nielsen, M. Hara-Chikuma, Aquaporin-9 facilitates membrane transport of hydrogen peroxide in mammalian cells, Biochem. Biophys. Res. Commun. 471 (2016) 191–197, https://doi.org/10.1016/j.bbrc.2016.01.153.
[52] M. Bertolotti, S. Bestetti, J.M. García-Manteiga, I. Medraño-Fernandez, A. Dal Mas, M.L. Malosio, R. Sitia, Tyrosine Kinase signal modulation: a matter of H2O2 membrane permeability? Antioxidants Redox Signal 19 (2013) 1447–1451, https://doi.org/10.1089/ars.2013.5330.
[53] E.W. Miller, B.C. Dickinson, C.J. Chang, Aquaporin-3 mediates hydrogen peroxide uptake to regulate downstream intracellular signaling, Proc. Natl. Acad. Sci. U.S.A. 107 (2010) 15681–15686, https://doi.org/10.1073/pnas.1005776107.
[54] A. Ledo, R.M. Barbosa, G.A. Gerhardt, E. Cadenas, J. Laranjinha, Concentration dynamics of nitric oxide in rat hippocampal subregions evoked by stimulation of the NMDA glutamate receptor, Proc. Natl. Acad. Sci. Unit. States Am. 102 (2005) 17483–17488, https://doi.org/10.1073/pnas.0503624102.
[55] A. Philippides, P. Husbands, M. O'Shea, Four-dimensional neuronal signaling by nitric oxide: a computational analysis, J. Neurosci. 20 (2000) 1199–1207, https://doi.org/10.1523/jneurosci.20-03-01199.2000.
[56] S.A.M. van Stroe-Biezen, F.M. Everaerts, L.J.J. Janssen, R.A. Tacken, Diffusion coefficients of oxygen, hydrogen peroxide and glucose in a hydrogel, Anal. Chim. Acta 273 (1993) 553–560, https://doi.org/10.1016/0003-2670(93)80202-V.
[57] R.F. Eich, T. Li, D.D. Lemon, D.H. Doherty, S.R. Curry, J.F. Aitken, A.J. Mathews, K. A. Johnson, R.D. Smith, G.N. Phillips, J.S. Olson, Mechanism of NO-induced oxidation of myoglobin and hemoglobin, Biochemistry 35 (1996) 6976–6983, https://doi.org/10.1021/bi960442g.
[58] L.F. Agnati, D. Guidolin, M. Guescini, S. Genedani, K. Fuxe, Understanding wiring and volume transmission, Brain Res. Rev. 64 (2010) 137–159, https://doi.org/10.1016/j.brainresrev.2010.03.003.
[59] L.F. Agnati, K. Fuxe, Volume transmission as a key feature of information handling in the central nervous system possible new interpretative value of the Turing's B-type machine, Prog. Brain Res. 125 (2000) 3–19, https://doi.org/10.1016/S0079-6123(00)25003-6.
[60] M. Spanos, J. Gras-Najjar, J.M. Letchworth, A.L. Sanford, J.V. Toups, L.A. Sombers, Quantitation of hydrogen peroxide fluctuations and their modulation of dopamine dynamics in the rat dorsal striatum using fast-scan cyclic voltammetry, ACS Chem. Neurosci. 4 (2013) 782–789, https://doi.org/10.1021/cn4000499.